

# Estimation of land surface temperature and distribution across Land use/land cover in response to coal mining activity in V. D. Yelevsky coal mine area – Russia

Al-shateri Hoshmand Ahmed Azeez<sup>1</sup>

Received 22 February 2021; accepted 1 October 2021; published 10 May 2022.

Land surface temperature is an important factor in many areas, such as global climate change, hydrological, geophysical, biophysical, and land use land cover. This study attempts to retrieve the current statue of V. D. Yelevsky coal mine area in Russia and estimate Land surface temperature in the area of the years of 2006, 2010, and 2019. Furthermore, the study shows the distribution of land surface temperature among land use land cover in the area and implies spatial correlation between land surface temperature and normalized different vegetation index by using Landsat 5 and Landsat 8. The results show that the statue of coal mine portion has increased from 43.89 km<sup>2</sup> in 2006 to 111.40 km<sup>2</sup> in 2019. Also, in the three periods maximum images temperature was recorded in coal mine area (32.05°C in 2006, 31.24°C in 2010 and 32.81°C in 2019), while minimum temperature value of land use land cover types varies among the years. In 2006 minimum value of 12.36°C recorded in water bodies area, 12.36°C across forest area, and again 18.41°C across water bodies in 2019. Consequently, the average land surface temperature of overall area for the three observed years has increased from 18°C to 22.2°C, it means that changes of land surface temperature have been observed from the period of 2006 to 2019. On the other hand, the results show that land surface temperature and normalized different vegetation index for the three study years have strong negative correlations with  $R$  square value of ( $R^2 = 0.93$  in 2006,  $R^2 = 0.99$  in 2010 and  $R^2 = 0.87$  in 2019) respectively. **KEYWORDS:** Coal mine; remote sensing; Landsat 5 and 8; land surface temperature; normalized difference vegetation index.

**Citation:** Al-shateri Hoshmand Ahmed Azeez, (2022), Estimation of land surface temperature and distribution across Land use/land cover in response to coal mining activity in V. D. Yelevsky coal mine area – Russia, *Russ. J. Earth. Sci.*, 22, ES2005, doi:10.2205/2021ES000778.

## 1. Introduction

Mining is the extraction or removal of coal from the beneath of the Earth. Coal can be extracted from either by open pit mining or by underground mining. Coal is the prime energy resource in most

countries, 60% of them located in threecountries: the United States, Russia, and China. Coal is one of the largest sources of energy in Russia. The prominence of coal power in Russia has been declining since 1990. Russia is the fifth largest consumer of coal in the world and is the sixth largest producer of coal. The total coal reserves in Russia estimated at 1.1 trillion tons, which are located in 22 coal basins and 129 separate deposits. Russia's coal industry annually produces 350 million tons of coal which is provided not only the Russian Federation needs but is exported as well. The biggest coal reserves are in the USA, Russia, China, and India.

<sup>1</sup>Surveying Department, Kalar Technical College, Sulaimani Polytechnic University, Sulaimani, Kurdistan-Iraq

Mineral resources hold a significant position in economic development as a result of their importance for both raw materials and energy [Hu *et al.*, 2014; Xiao *et al.*, 2016, 2018]. The demand for mineral resources has increased significantly with the growth of industry and urbanization, leading to a greater need for mining.

While coal forms an important energy source for all the country around the world, its environmental impact cannot be ignored and has been a challenge for all. Coal mining is associated with number of environmental issues, some of its prime impacts are: (1) Emission of many toxic gases, such as carbon monoxide (CO), carbon dioxide (CO<sub>2</sub>), sulfur oxides (SO<sub>x</sub>), methane (CH<sub>4</sub>), and nitrogen oxides (NO<sub>x</sub>). Among these noxious gases, CO<sub>2</sub> and CH<sub>4</sub> contribute to global warming; (2) Geomorphic effects, include land subsidence, surface cracks, faults, and other geologic structures, (3) Temperature increment of surrounding areas, desiccation of forests, lowering of water quality [Ritesh Kumar, 2019].

LST is an important factor in many areas of studies, such as global climate change, hydrological and agricultural processes, and urban land use/land cover. Calculating LST from remote sensed images is needed since it is an important factor controlling most physical, chemical, and biological processes of the Earth [Becker *et al.*, 1990]. There is a growing awareness among environmental scientists that remote sensing can and must play a role in providing the data needed to assess ecosystems conditions and to monitor change at all special scales [Ustin *et al.*, 2004]. Remote sensing instruments are key players to study and map land surface temperature (LST) at temporal and spatial scales [André *et al.*, 2015]. Remote sensing methodology requires less time and lower cost than field methods to investigate various phenomena on the land surface [Niu *et al.*, 2015]. The advantages of using remote sensing methodology are the repetitive and consistent coverage, high resolution and evaluation of land surface characteristics [Owen *et al.*, 1998]. Thermal infrared (TIR) data in remote sensing can help us obtain quantitative information of surface temperature.

Many researchers showed that the surface temperature of the work confirmed from Landsat-5/8 [Amiri *et al.*, 2009; Avdan and Jovanovska, 2016; Guo *et al.*, 2012; Mallick *et al.*, 2012; Xiao *et al.*, 2016].

LST, calculated from remote sensing data, is used in many areas of science; such as; hydrology, agriculture, climate change, urban planning, forestry, oceanography etc. Obtaining surface temperatures and using them in different analysis is important to determine the problem associated with the environment [Orhan *et al.*, 2014].

The present study focus on this present study was conducted in V. D. Yelevsky coal mine area in the Kuzbass region of Siberia, Russia, which is operated by SUEK. Recently produced a total of 1.6 million t of coal in August 2019, and setting a world record for monthly productivity in the coal industry.

In the present study, heterogeneous surface temperature and NDVI of V. D. Yelevsky coal mine area in Russia were calculated, by using Multi temporal thermal image series were acquired by Landsat-5 TM/8-OLI for the period of (8th September 2006 “04:59 am”, 25th August 2010 “05:01 am” and 27th August 2019 “05:05 am”).

The aim of the study firstly is to generate statue of coal mine in the area and estimate LST, then analyze distribution of LST across LU/LC types. In addition, indicate correlation between LST and NDVI in the area through the period of 2006, 2010 and 2019.

## 2. Material and Methods

### 2.1. Study Area

The V. D. Yelevsky coal mine has been chosen as the study area, which is located in Kuzbas region of Siberia, Russia. The process of mining in the area nearly started in 1991. Kuzbass is located in southwestern Siberia, where the West Siberian Plain meets the South Siberian mountains. The region, which covers an area of 95,500 square kilometers (36,900 sq mi), shares a border with Tomsk region in the north, Krasnoyarsk Krai and the Republic of Khakassia in the east, the Altai Republic in the south, and with Novosibirsk region and Altai Krai in the west. The population in the region recorded during the 2019 census was 564,383.

The study area is located in (54°11'29.60"N) latitude and (87°9'28.77"E) longitude. The area has an altitude of 278 m Figure 1. The total economy of the region is highly dependent on coal mining.

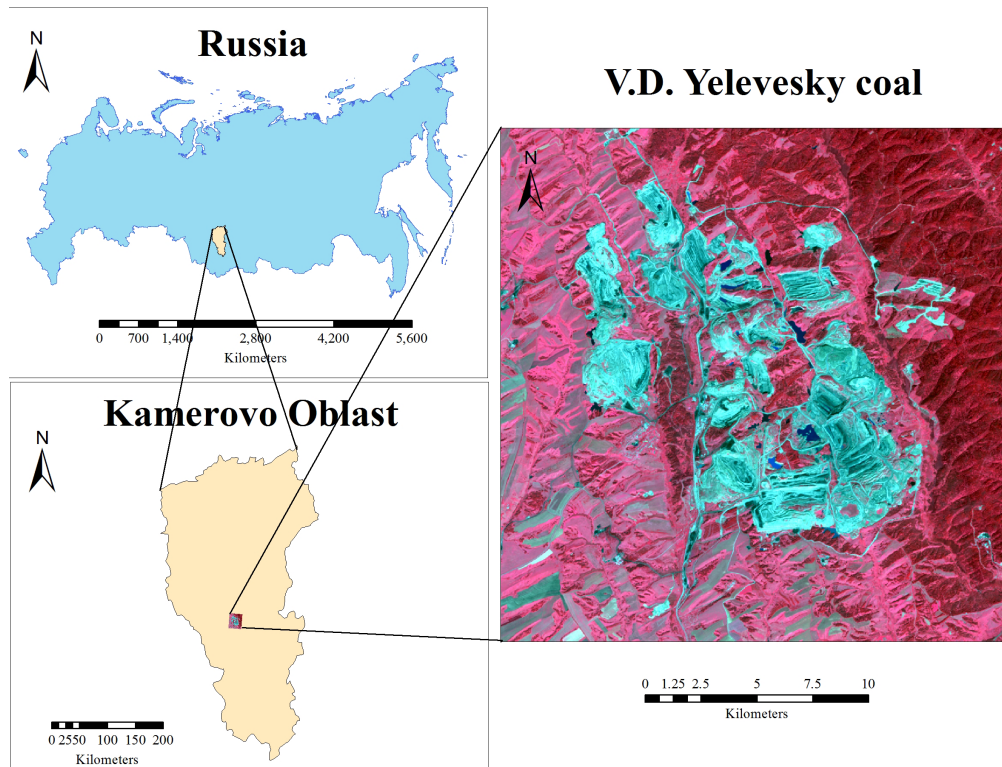


**Figure 1.** Geographic location map of the V. D. Yelevesky coal mine area.

Extraction of coking coal from the coal enriching plant is the main industry of the region. The present study area cover about 616 km<sup>2</sup> and the predominant features of the territory are (mine area, forest, water bodies in the form of small basin, road, agriculture and vegetation). The V. D. Yelevesky coal mine area is bounded on the west by density forest and on the east by agriculture.

## 2.2. Geography and Climate

The Kemerovo Region – Kuzbass is located in the southeast of Western Siberia, Russia. Climate is continental with average temperatures between  $-10$  and  $-13^{\circ}\text{C}$  in January and between  $18$  and  $20^{\circ}\text{C}$  in July. The main river is the Tom'. Annual precipitation amounts to 300–500 mm. Soils are podzolic. Kuzbass has the largest deposits of coal in Russia accounting for a quarter of all energy resources of the country.

Agriculture accounts for about 4% of the regional gross domestic product. The local climate supports cultivation of crops (wheat, oats, barley), potatoes, and vegetables. Dairy and beef farming, as well

as pig and poultry farming, are well developed in the region. The Agro-industrial sector supplies the entire region with grain, potatoes, vegetables and eggs, but falls short of demand for meat and dairy products. The daylight hours increase from 7 hours in the middle of December to 17 hours 30 minutes in the middle of June.

## 2.3. Image Acquisition and Pre-Processing

Landsat TM (2006 and 2010), and OLI (2019), digital elevation model SRTM (Shuttle Radar Topography Mission) (2014), and Sentinel-2A Satellite sensor data were obtained from United State Geological Survey (USGS). In addition Google Earth images collected to assess accuracy assessment. All sets of used data are pre-processed. Thermal band (Band 6 for TM sensor and Band 10 for OLI/TIRS sensor) were used to calculate and estimate land surface temperature. In addition Normalized Difference Vegetation Index (NDVI) for each year were computed. For processing the data, Arc GIS 10.2 and ENVI software 5.1 has been used for the study.

## 2.4. Method for Land Use/Land Cover Classification

Landsat TM (Thematic Mapper) data of the 2006 and 2010, band no. 1–5 and 7 have been used for land use mapping, band no. 6 not used as it is a thermal band whereas from Landsat OLI (Operational Land Imager) data only band no. 1–7 has been used. Supervised image classification technique with maximum likelihood method has been used to show the coal mine and land use/land cover in the area. To get six different land use class huge number of signature has been collected. Total 1921 signatures from all three images are collected and merged to detect each land use class properly.

## 2.5. Method for Accuracy Assessment of Land Use Classification

Accuracy is done to see how closely the results relate to the true values and gives the qualitative collection of information from the obtained satellite data. To assess the accuracy assessment of supervised image classification an error matrix of referenced data has been done by using ground truth ROI's to get the user's and producer's accuracy. For calculation of those total 11508 sample sites has been selected from Google earth images and Sentinel-2A, then match them with the LU/LC map for verification. The percentage of matched no. of sites to total no of sites has been calculated using the following formula, which are called overall accuracy (OA)

$$OA = \frac{\sum DV}{N}.$$

Accuracy for every individual land use classes are also calculated in the same manner. There are two approaches one is user's accuracy another is producer's accuracy. These two types of accuracy can be calculated by two formulae as mentioned below. The user's accuracy is calculated by dividing the matched no. of sites of an individual land use category by total sites of the same category [*Story and Congalton, 1986*] multiplied by 100. The measures of commission error of the user's accuracy indicate the probability of a site classified in a category that actually available in the same category [*Khorram, 1999; Lunetta et al., 2001; Pal and Ziaul, 2017;*

*Zhou et al., 1998*]. Whereas, the producer's accuracy is calculated by dividing the no. of matched sites to the total no. of sites evolved from referenced data multiplied by hundred. It measures how well an area has been categorized. The omission error (OE) of the producer's accuracy (PA) refers proportion of observed sites on ground are not classified in referenced map. By using the following formula's producer's accuracy and user's accuracy (UA) are obtained:

$$OE = \frac{\sum DVC}{CT} \times 100;$$

$$PA = \frac{DVC}{CT} \times 100\%;$$

$$CE = \frac{\sum DVR}{RT} \times 100;$$

$$UA = \frac{DVR}{RT} \times 100\%,$$

where DVC – diagonal value column; CT – column total; CE – commission error; DVR – diagonal value row; RT – row total.

Another method of measuring the accuracy is the Kappa coefficient ( $K$ ) [*Foody, 1992; Ma and Redmond, 1995*]. In this study to get the accuracy of the maps Kappa coefficient are also computed for land use map of all three years. For calculation of Kappa summation of the diagonal value (Ra) are calculated the diagonal value and divided it with the total no. of observed points ( $N$ ) from the result summation of expected frequency (ef) are subtracted and then it has been divided by subtraction of summation of expected frequency from 1. Where, ef is calculated by dividing the multiplication of the row sum (RS) and column sum (CS) with observed no. of sites ( $N$ ). The value of Kappa varies from 0 to 1. Where, 0 (zero) represents the worst and 1 (one) represents the best. But these two extreme values come due to chance only. Kappa can be gives negative values but only in rare case, in general the maximum value cannot exceed 1 (one) and the minimum cannot lower than 0 (zero). Kappa is more sophisticated measure than overall accuracy and it gives more inter class discrimination in result [*Foody, 1992; Ma and Redmond, 1995; Pal and Ziaul, 2017*]. The value

of Kappa is expressed as percentage (%). Kappa coefficient is derived by the following formula:

$$K = \frac{\left(\frac{\sum a}{N}\right) - \sum ef}{1 - \sum ef},$$

where  $a$  = Diagonal frequency;  $N$  = Total number of frequency;  $ef$  = Expected frequency. Expected frequency ( $ef$ ) can be calculated as the following formula

$$ef = \frac{RT \times CT}{N}.$$

So, kappa always gives result from 0 to 1. The value 1 means the perfectly accurate and when it is decreasing toward 0, it loses their perfectness. Different scholars have different interpretation regarding the value of kappa coefficient. Suggestion made by that kappa's value less than 0.40 represent very pore kind of accuracy, it is fare when value 0.40 to 0.55, value from 0.55 to 0.70 represent good accuracy, very good represented by the value from 0.70 to 0.85, value beyond 0.85 represent the excellent accuracy between two images.

## 2.6. Method for Extraction of LST From Thermal Band of Satellite Imagery

Increase of temperature is a problem of the present world. To study the relation between increase of temperature with urbanization or the build-up area this paper tries to calculate the land surface temperature (LST) and to obtain the LST Landsat data from USGS are taken, which are freely available in the website. As only the thermal band are required for the extraction of LST data, the paper extract the thermal band (Band 6) from Landsat 5 TM for the year 1993 and 2009 and (Band 10 and Band 11) Landsat 8 OLI for the year 2015. For extraction of LST data from the thermal bands of the Landsat have to pass through six different steps using the ArcGIS 10.2 software. Following are those steps have been followed to extraction of land surface temperature from thermal bands of Landsat imageries [Ding and Shi, 2013]. In addition Estimation of land surface temperature in Landsat TM consists of two basic steps like converting Digital Number (DN) values to radiance and estimating radiant temperature from radiance which are

followed by all the literatures. But there are several methods of estimating land surface temperature. Some studies considered radiant temperature as land surface temperature. [Dontree, 2010] just follow the two basic steps to estimate land surface temperature.

### Conversion of digital number to radiance.

The first step to compute LST was conversion of the digital number in to radiance for TM sensor. Therefore, based on NASA model from metadata file, digital number of TM sensor was converted in to radiance value using the following equation.

$$L\lambda = \frac{L_{\max}\lambda - L_{\min}\lambda}{QCAL_{\max} - QCAL_{\min}} \times (QCAL - QCAL_{\min}) + L_{\min}\lambda,$$

where  $L\lambda$  – Spectral Radiance at the sensor's aperture;  $L_{\min}\lambda$  – the spectral radiance that is scaled to  $QCAL_{\min}$ ;  $L_{\max}\lambda$  – the spectral radiance that is scaled to  $QCAL_{\max}$ ;  $QCAL_{\min}$  – the minimum quantized calibrated pixel value (corresponding to  $L_{\min}\lambda$ );  $QCAL_{\max}$  – the maximum quantized calibrated pixel value (corresponding to  $L_{\max}\lambda$ );  $QCAL$  – the quantized calibrated pixel value.

OLI and TIRS thermal bands (Band 10) data was converted to Top of the Atmosphere (TOA) spectral radiance using the radiance rescaling factors provided in the metadata file. Hence, digital number for Landsat 8 imagery of thermal band is computed to generate radiance using equation below. The calculation of the spectral radiance ( $L\lambda$ ) has done using following equation [Landsat Project Science Office, 2002]:

$$L\lambda_{TOA} = ML \times QCAL + AL, \quad (1)$$

where  $L\lambda_{TOA}$  – TOA spectral radiance;  $ML$  – Band-specific multiplicative rescaling factor from the metadata;  $AL$  – Band-specific additive rescaling factor from the metadata;  $QCAL$  – the quantized calibrated pixel value.

### Conversion of radiance to At-Satellite temperature.

Once the spectral radiance  $L\lambda$  is computed, the brightness temperature at the satellite level can be directly calculated by either inverting Planck's radiance function for temperature [Sospedra et al., 1998]. Radiance value of TM sensor that is computed from (1) was converted in to At satellite temperature in Kelvin using Plank formula displayed in the following equation

$$T = \frac{K2}{\ln\left(\frac{K1}{L\lambda} + 1\right)}, \quad (2)$$

where:  $T$  – Effective at-satellite temperature in Kelvin;  $K2$  – Calibration constant 2;  $K1$  – Calibration constant 1;  $L$  – Spectral radiance.

[*Ghulam, 2010*], also followed the same equation. Several researchers also illustrated radiant temperature as surface temperature. Beside these two, [*Chander and Markham, 2003*] also used kinetic temperature as a final output of thermal remote sensing data. It didn't mention any necessity or use of emissivity or any other parameters for temperature correction. This method followed by the mentioned studies just used the radiant temperature rather than estimating land surface temperature through considering any surface parameters.

Similar to TM data, OLI/TIRS thermal band data was also converted from spectral radiance (derived using (1) to top of atmosphere brightness temperature using the thermal constants provided in the metadata file:

$$T = \frac{K2}{\ln\left(\frac{K1}{L\lambda_{TOA}} + 1\right)}, \quad (3)$$

where  $T$  – Top of atmosphere brightness temperature (K);  $L\lambda_{TOA}$  – TOA spectral radiance;  $K1$  – Band-specific thermal conversion constant from the metadata;  $K2$  – Band-specific thermal conversion constant from the metadata.

**Conversion of Kelvin to Celsius.**  $^{\circ}\text{C} = T - 273.15$ , where  $T$  = at satellite temperature computed from (2) and (3) for both TM and OLI/TIRS sensors. (this one show in the final by writing raster calculate form)

Normalized Difference Vegetation Index was used to calculate land surface emissivity of both study years. Hence, NDVI for Landsat TM, 2006, 2010 and Landsat OLI/TIRS, 2019 was computed. NDVI is obtained by using the following formula [*Townshend and Justice, 2007*]:

$$NDVI = \frac{NIR - RED}{NIR + RED},$$

where NIR means near infrared band and  $R$  means red band. For LANDSAT TM data band 3 and 4 and for LANDSAT OLI data band 4 and 5 were used to calculate NDVI. NDVI is used to indicate

the green space of an area. The value of NDVI varies from (negative) 1 to (positive) +1. Values from 0 to (positive) +1 indicate vegetation cover and the value close to 1 indicate high density of vegetation.

**Proportion of Vegetation (PV) can be calculated.**

$$PV = \left( \frac{NDVI - NDVI_{\min}}{NDVI_{\max} - NDVI_{\min}} \right)^2,$$

where  $PV$  – Proportion of vegetation;  $NDVI_{\min}$  – minimum value of NDVI;  $NDVI_{\max}$  – maximum value of NDVI.

**Retrieving of land surface emissivity:**

Land surface emissivity ( $LSE$ ) is retrieved after NDVI has calculated. Land surface emissivity of the two sensor imagery was calculated via the following formula

$$LSE = 0.004 \times PV + 0.986.$$

**Land surface temperature (LST).**

$$LST = BT + \frac{W \times BT \times P \times \ln(LSE)}{P},$$

where  $BT$  – at satellite temperature;  $W$  – wavelength of emitted radiance.

**Conversion of LST data to centigrade scale.** After preparing all the LST data value of the temperature has been come in the Kelvin scale. As this scale is not a commonly used format we need to convert this Kelvin (K) data to the Celsius (C) for simplification and widely understandable of the temperature data. The value 273.15 has subtracted from the data for every pixel with GIS, as the value of Kelvin (K) scale is 273.15 more than the Celsius scale.

### 3. Results and Discussion

#### 3.1. Areal Distribution of Land Use/Land Cover Types

Firstly, to detect coal mine in the area, and areal distribution of land use/ land cover types, LU/LC map generated. LU/LC types for the three years (2006, 2010 and 2019) has been categorized into six classes, such as: Forest, Water bodies, Coal

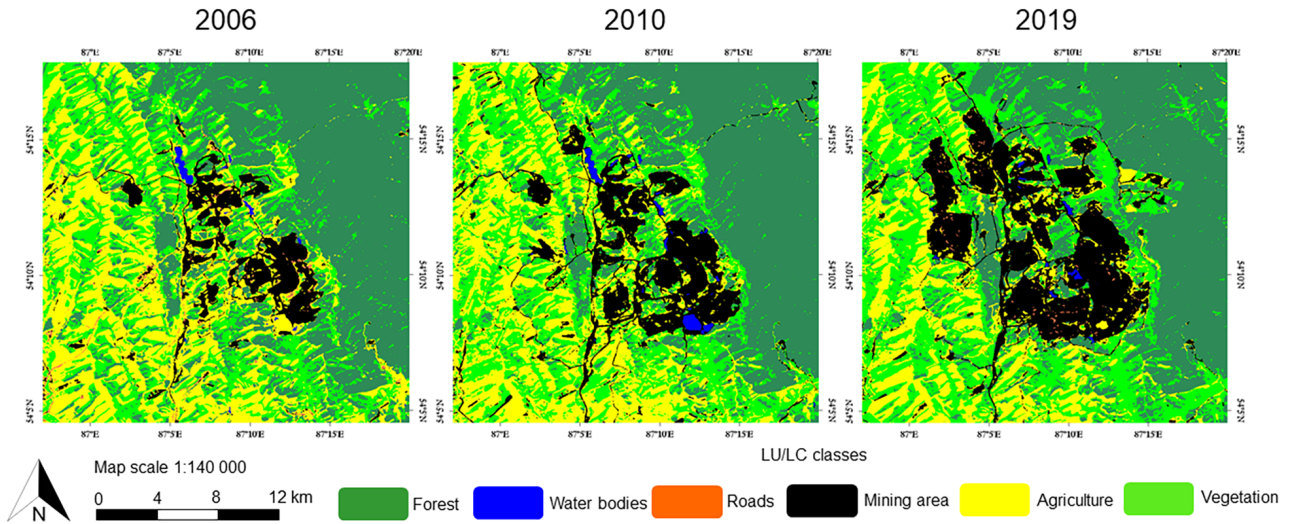


Figure 2. Land use land cover map of the area.

Table 1. Accuracy Assessment of Land Use/Land Cover Classes

Classes	Classified image, 2006		Classified Image, 2010		Classified Image, 2019	
	Producer's accuracy (%)	User's accuracy (%)	Producer's accuracy (%)	User's accuracy (%)	Producer's accuracy (%)	User's accuracy (%)
Forest	91.03	97.26	95.58	93.10	97.53	94.61
Water bodies	100.00	100.00	87.50	100.00	100.00	100.00
Road	27.27	100.00	12.50	50.00	4.00	9.09
Mining area	100.00	96.18	98.91	91.92	94.62	90.72
Agriculture	97.91	91.67	83.61	85.00	83.71	89.76
Vegetation	84.95	84.95	74.19	74.19	90.00	75.90
Overall accuracy	93.41%		88.33%		88.69%	
Kappa coefficient	0.91		0.85		0.85	

mine, Road, Agriculture and Vegetation (Figure 2). The accuracy assessment for land use classification was analyzed by using Google Earth Imagery and Sentinel-2A image. The overall accuracy (%) for classified images are; for the year 2006 is 93.41, for the year 2010 is 88.333 and for 2019 is 88.69. The reliability of the result was derived with the help of Kappa coefficient. The values of Kappa coefficient are 0.91, 0.85 and 0.85 for the years 2006, 2010 and 2019 respectively. The land use distribution in V. D. Yelovsky coal mine is illustrated in Table 1. By comparing area percentage values of different land use classes between images, it can be concluded that land use types of the study area

were significantly converted in the 13-years period. Table 2 shows that the coal mine and vegetation increased. However, forest, road, agriculture and water bodies were decreased during the time. The main changes include conversion of agriculture to coal mine.

**3.2. Spatial Distribution NDVI and Correlation With LST** Method for calculate spatial indices (NDVI) and correlation with LST has been calculated using Landsat data with the help of ArcGIS software (version 10.2). NDVI was used to present the relationship between LST and vegetation area in this study by linear regression cor-

**Table 2.** Areal Distribution of Land Use/Land Cover Classes

LULC Classes	Areal LU/LC 2006		Areal LU/LC 2010		Areal LU/LC 2019	
	Area, km <sup>2</sup>	%	Area, km <sup>2</sup>	%	Area, km <sup>2</sup>	%
Forest	245.40	39.87	216.93	35.24	215.66	35.04
Water bodies	1.94	0.32	3.66	0.59	1.18	0.19
Road	4.67	0.76	1.55	0.25	1.46	0.24
Mining area	43.89	7.13	73.25	11.90	111.40	18.10
Agriculture	168.01	27.30	156.27	25.39	108.35	17.60
Vegetation	151.60	24.63	163.85	26.62	177.46	28.83

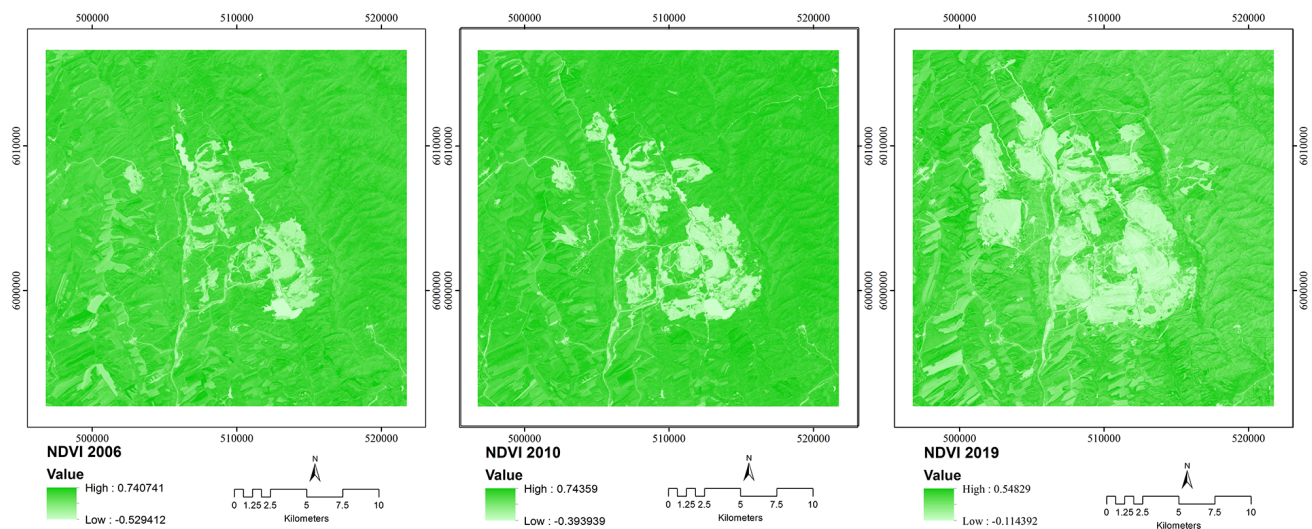


**Figure 3.** Normalized difference vegetation index 2006, 2010 and 2019.

relation. The value of NDVI ranges from +1 to -1 where positive value indicates high vegetation cover and negative value indicates less vegetated area. The higher vegetation cover helps to lowering the LST. So, there is a negative and strong correlation between LST and NDVI. The spatial distribution of NDVI values from the Landsat TM image in (2006, 2010 and 2019) can be seen in Figure 3.

The 2006 NDVI values are in the range of -0.53 to 0.74, having a mean value of 0.44, while more index was in forest area and less index was in vegetation area. The 2010 NDVI values are in the range of -0.39 to 0.74, having a mean value of 0.513, while more index was in agricultural area and less index was in water bodies. Moreover the 2019 NDVI values are in the range of -0.11 to 0.55, having a mean

value of 0.276, while more index was in agricultural area and less index was in water bodies Table 3.

So most of the area have high NDVI shown in dark green, but from the analysis, it is clear that there is decreasing trend in vegetation cover. In the figures below, (Figure 4) shows that, LST and NDVI for the three study years have strong negative correlation with  $R$  square value of ( $R^2 = 0.93$  in 2006,  $R^2 = 0.99$  in 2010 and  $R^2 = 0.87$  in 2019) respectively.

### 3.3. Land Surface Temperature Change Analysis

The result of the research shows the status of V. D. Yelevisky coal mining area, land cover classification and estimate it's surface temperature across

**Table 3.** Normalized Different Vegetation Index Land Use Land Cover Classes 2006, 2010 and 2019

Classes	NDVI, 2006				NDVI, 2010				NDVI, 2019			
	Min	Max	Mean	STD	Min	Max	Mean	STD	Min	Max	Mean	STD
Forest	-0.35	0.74	0.48	0.06	0.19	0.74	0.59	0.05	-0.02	0.47	0.30	0.04
Water bodies	-0.44	0.22	-0.17	0.06	-0.39	0.08	-0.17	0.10	-0.11	-0.01	-0.05	0.02
Road	-0.21	0.69	0.34	0.10	-0.05	0.39	0.10	0.08	-0.02	0.33	0.10	0.05
Coal mine	-0.45	0.66	0.10	0.13	-0.33	0.63	0.14	0.15	-0.11	0.39	0.08	0.06
Agriculture	-0.45	0.72	0.42	0.13	-0.02	0.74	0.51	0.06	0.02	0.48	0.27	0.06
Vegetation	-0.53	0.73	0.50	0.07	0.07	0.74	0.60	0.05	0.15	0.55	0.37	0.03

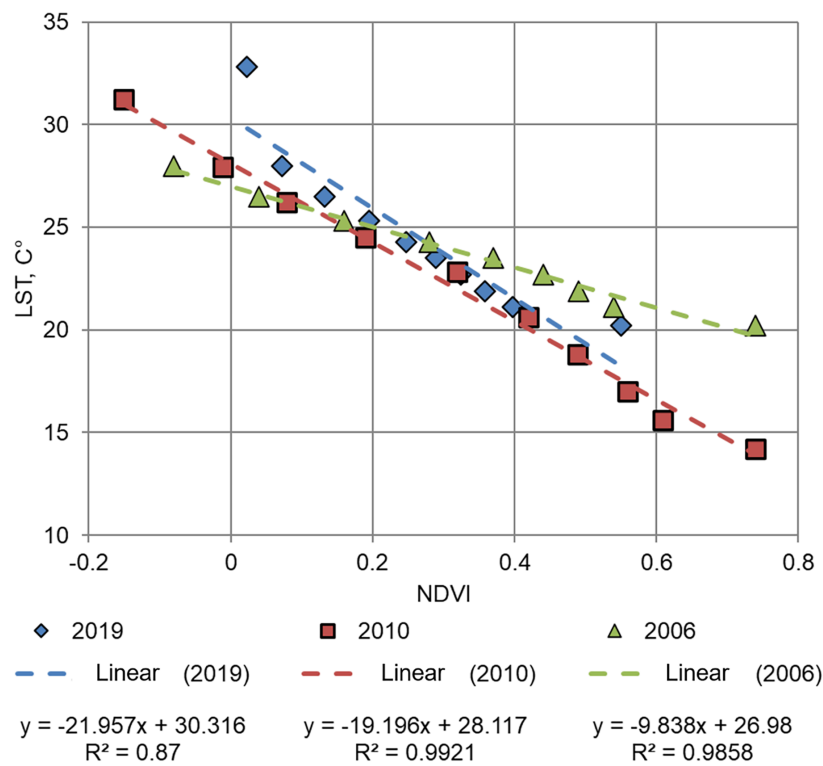


**Figure 4.** LST and NDVI Correlation 2006, 2010 and 2019.

the area compared with other LULC types. The distribution of surface temperature follows the distribution of land cover. This means that the difference of surface temperature because of differences in the thermal capacity of the object. All observations in 2006, 2010 and 2019, showed that there was overall warmer surface temperatures in the areas of development by human activity, such as mining coal.

Land surface temperature was derived from Landsat imagery (TM and OLI/TIRS). LST was es-

timated using conversion of radiance to At satellite brightness temperature and spectral emissivity. The spatial distribution of surface temperature of the 2006, 2010 and 2019 images are shown in the Figure 5. There are some differences among the three-period LSTs. Surface temperature of 2006 LST image ranged from 12.36 to 32.05°C (mean of 22°), and surface temperature of the 2010 LST image ranged from 12.36 to 31.24 °(mean of 17.77°). In addition surface temperature of the 2019 LST image ranged from 18.41 to 32.81° (mean of 22.2°).

**Table 4.** Distribution of Surface Temperature in the Area

Classes	LST, 2006				LST, 2010				LST, 2019			
	Min	Max	Mean	STD	Min	Max	Mean	STD	Min	Max	Mean	STD
Forest	13.78	23.68	16.63	0.87	12.36	21.06	14.19	0.74	18.85	25.56	20.30	0.62
Water bodies	12.36	23.25	14.19	1.03	13.78	23.68	15.97	1.19	18.41	25.17	19.79	0.89
Road	15.18	25.83	19.35	1.35	14.71	29.60	21.74	2.34	19.51	31.57	24.29	1.76
Coal mine	13.78	32.05	21.09	2.25	13.31	31.24	21.13	2.68	18.73	32.81	24.40	1.78
Agriculture	12.84	26.25	18.62	1.30	13.31	26.67	17.49	1.21	19.21	27.93	22.80	0.91
Vegetation	14.25	24.55	18.27	1.11	12.36	24.11	16.13	1.10	19.14	25.65	21.72	0.76

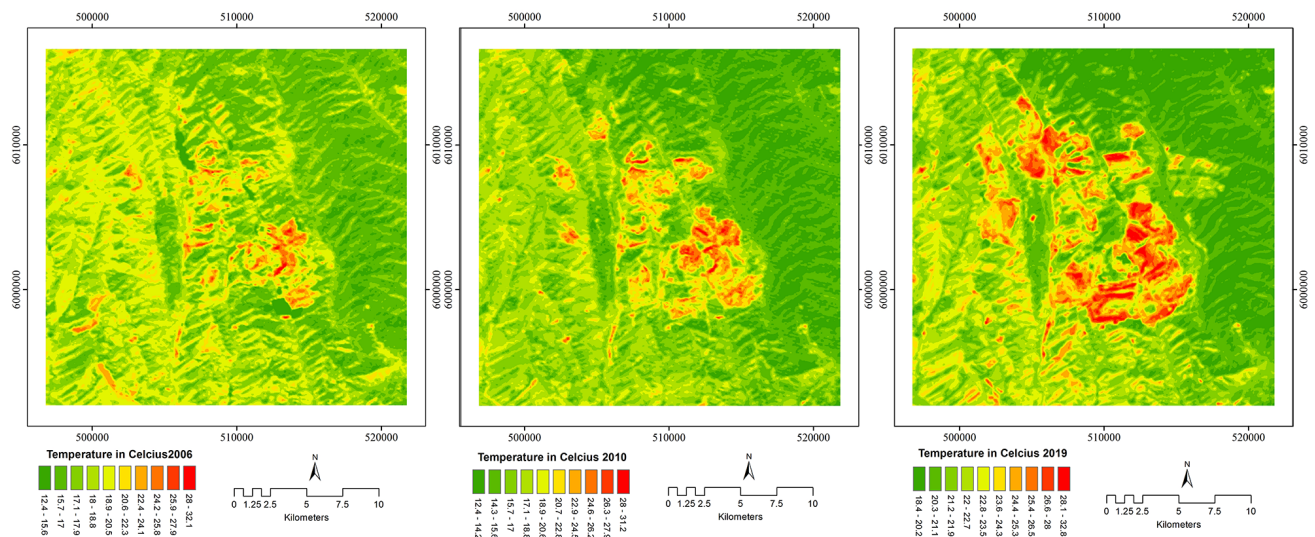


**Figure 5.** Land surface temperature of the study area.

Across the study area zonal statistics has been made to represent the variations and spatial distribution of LST between coal mine area and other LU/LC types. Table 4 shows that the surface temperature each land cover increases dramatically.

In the three period images maximum temperature was recorded in coal mine area (32.05°C in 2006, 31.24°C in 2010 and 32.81°C in 2019), while minimum temperature value of LU/LC types varies among years. In 2006 minimum value of 12.36°C recorded in water bodies area, 12.36°C across forest area, and again 18.41°C across water bodies in 2019. Furthermore the mean value of temperature 17.91°C recorded in 2006, 16.04°C in 2010, and 21.09°C in 2019. Therefore, the average LST of overall area for the three observation years has in-

creased from 17.91°C to 21.09°C, it means change of LST has been observed from the period of 2006–2019. Accordingly, in 2006, 2010 and 2019 coal mine area exhibit the highest LST. Moreover according to the results it is observed that coal mine excepting its increase, effected increasing temperature of other LU/LC types. Figure 5 show the surface temperature of the study area.

#### 4. Conclusion

In this study land surface temperature in V. D. Yelevsky coal mine area investigated. In addition the spatial distribution of LU/LC, land

surface temperature and NDVI was analyzed. The study use TM, 2006, 2010 and OLI/TIRS, 2019 Landsat images and images has classified in to six major LU/LC categories. The finds of the study indicates rise of temperature due to mining activity and significant expansion of its areal distribution in the area, in the last 13 years. The portion of coal mine in LU/LC types recorded highest value of temperature in the three images (32.05°C in 2006, 31.24°C in 2010 and 32.81°C in 2019), while minimum temperature value of LU/LC types varies among years. In 2006 minimum value of 12.36°C recorded in water bodies area, 12.36°C across forest area, and again 18.41°C across water bodies in 2019. More over the mean value of temperature in the area has increased from 18°C to 22.2°C, it means change of LST has been observed from the period of 2006–2019.

With regard to NDVI, According to the result of the study, the 2006 NDVI values were in the range of  $-0.53$  to  $0.74$ , in 2010 NDVI values were in the range of  $-0.39$  to  $0.74$ , and  $-0.11$  to  $0.55$  in 2019. Results implies it has strong negative correlation between LST and NDVI. Correlation with  $R$  square value of ( $R^2 = 0.93$  in 2006,  $R^2 = 0.99$  in 2010 and  $R^2 = 0.87$  in 2019) respectively.

Coal mine activity is the factor for changes in land use/land cover and increase of LST. The increasing trend of coal mining area highly responsible for significant increase of land surface temperature in the Region. As vegetated areas are converting into coal mine areas, so there should be implementation of some management policies like increase of green space. In above mentioned analysis, it's clear that if vegetation gets destroyed due to mining purpose, pollution will be spreading in surrounding areas, also if it is going to continue, ultimately the land will be polluted and temperature rise will be high. The government, mining company and also local people should take action, plan for protecting the area by plantation.

**Conflict of Interests:** None.

**Acknowledgment.** The author is grateful to the reviewers and editors of the Russian Journal of Earth Sciences for their help in publishing. Also, the author would like to thank Prof. Dr. Andrian Batugin and Dr. Alexander Manevich for their help in various ways.

## References

- Amiri, R., Q. Weng, et al. (2009), Spatial-temporal dynamics of land surface temperature in relation to fractional vegetation cover and land use/cover in the Tabriz urban area, Iran, *Remote Sensing of Environment*, 113, No. 12, 2606–2617, [Crossref](#)
- André, C., C. Ottle, et al. (2015), Land surface temperature retrieval over circumpolar Arctic using SSM/I–SSMIS and MODIS data, *Remote Sensing of Environment*, 162, 1–10, [Crossref](#)
- Avdan, U., G. Jovanovska (2016), Algorithm for automated mapping of land surface temperature using Landsat 8 Satellite data, *Journal of Sensors*, 2016, 1–8, [Crossref](#)
- Becker, F., Li Zhao-Liang (1990), Towards a local split window method over land surfaces, *International Journal of Remote Sensing*, 11, No. 3, 369–393, [Crossref](#)
- Chander, Gwanesh, Brian Markham (2003), Revised Landsat-5 TM Radiometric calibration procedures and post calibration dynamic ranges, *IEEE Transactions on Geoscience and Remote Sensing*, 41, No. 11, 2674–2677, [Crossref](#)
- Ghulam, A. (2010), @empty
- Ding, Haiyong, Wenzhong Shi (2013), Land-use/land-cover change and its influence on surface temperature: A case study in Beijing city, *International Journal of Remote Sensing*, 34, No. 15, 5503–5517, [Crossref](#)
- Dontree, S. (2010), Relation of land surface temperature (LST) and land use/land cover (LULC) from Remotely sensed data in Chiang Mai – Lamphun basin, *Online proceedings conference paper* p. 23–26, SEGA, Hanoi, Vietnam.
- Foody, G. M. (1992), On the compensation for chance agreement in image classification accuracy assessment, *Photogrammetric Engineering and Remote Sensing*, 58, No. 10, 1459–1460, [Crossref](#)
- Guo, Z., S. D. Wang, et al. (2012), Assess the effect of different degrees of urbanization on land surface temperature using remote sensing images, *Procedia Environmental Sciences*, 13, 935–942, [Crossref](#)
- Hu, Zhenqi, Yang Guanghua, et al. (2014), Farmland damage and its impact on the overlapped areas of cropland and coal resources in the eastern plains of China, *ELSEVIER, Recourses, Conservation and Recycling*, 86, [Crossref](#)
- Khorrarn, S. (1999), *Accuracy Assessment of Remote Sensing-Derived Change Detection*, American Society for Photogrammetry and Remote Sensing, Bethesda, MD.
- Landsat Project Science Office (2002), *National Aeronautics and Space Administration, Landsat 7 Science Data User's Handbook*, 186 pp. NASA's Goddard Space Flight Center, Greenbelt. ([http://landsathandbook.gsfc.nasa.gov/pdfs/Landsat7\\_Handbook.pdf](http://landsathandbook.gsfc.nasa.gov/pdfs/Landsat7_Handbook.pdf))

- Lunetta, R. S., J. Iames, et al. (2001), An assessment of reference data variability using a virtual field reference database, *Photogrammetric Engineering and Remote Sensing*, 63, No. 6, 707–715, **Crossref**
- Ma, Z., R. L. Redmond (1995), Tau coefficients for accuracy assessment of classification of remote sensing data, *Photogrammetric Engineering and Remote Sensing*, 61, No. 4, 435–439. (Corpus ID:126955874)
- Mallick, J., C. K. Singh, et al. (2012), Land surface emissivity retrieval based on moisture index from LANDSAT TM satellite data over heterogeneous surfaces of Delhi city, *International Journal of Applied Earth Observation and Geoinformation*, 19, 348–358, **Crossref**
- Niu, C., A. Musa, Y. Liu (2015), Analysis of soil moisture condition under different land uses in the arid region of Horqin sandy land, northern China, *Solid Earth*, 6, 1157–1167, **Crossref**
- Owen, T. W., T. N. Carlson, R. R. Gillies (1998), An assessment of satellite remotely-sensed land cover parameters in quantitatively describing the climatic effect of urbanization, *International Journal of Remote Sensing*, 19, No. 19, 1663–1681, **Crossref**
- Orhan, O., S. Ekercin, F. Dadaser-Celik (2014), Use of Landsat land surface temperature and vegetation indices for monitoring drought in the salt lake basin area, Turkey, *The Scientific World Journal*, 2014, 1–11, (Article ID 142939) **Crossref**
- Pal, S., S. Ziaul (2017), Detection of land use and land cover change and land surface temperature in English Bazar urban center, *The Egyptian Journal of Remote Sensing and Space Science*, 20, No. 1, 125–145, **Crossref**
- Ritesh, Kumar, Sharma Sadanand, et al. (2019), Environmental issues of coal mines and it's allied industries: Suggestive measures for root level remedies, *International conference and exhibition on energy and environment: Challenges and Opportunities 1*, p. 332–339, Vigyan Bnawan, New Delhi, India. (<http://cimfr.csircentral.net/id/eprint/2040>)
- Story, M., R. G. Congalton (1986), Accuracy assessment: A user's perspective, *Photogrammetric Engineering and Remote Sensing*, 52, No. 3, 397–399, **Crossref**
- Sospedra, F., V. Caselles, E. Valor (1998), Effective wavenumber for thermal infrared bands-application to Landsat-TM, *International Journal of Remote Sensing*, 19, No. 11, 2105–2117, **Crossref**
- Townshend, J. R. J., C. O. Justice (2007), Analysis of the dynamics of African vegetation using the normalized difference vegetation index, *International Journal of Remote Sensing*, 7, No. 11, 1435–1445, **Crossref**
- Ustin, S. (2004), *Manual of Remote Sensing Remote Sensing for Natural Resource Management and Environmental Monitoring, Vol. 4, Third edition*, 768 pp. John Wiley & Sons, California.
- Xiao, Wu., Jiale Chen, et al. (2018), Inversion and analysis of maize biomass in coal mining subsidence area based on UAV images, *Transactions of the Chinese Society for Agricultural Machinery*, 49, No. 8, 169–180, **Crossref**
- Xiaoxiao, Li, Li Wenwen, et al. (2016), Remote sensing of the surface urban heat island and land architecture in Phoenix, Arizona: Combined effects of land composition and configuration and cadastral-demographic-economic factors, *Remote Sensing of Environment*, 174, 233–243, **Crossref**
- Zhou, Q., M. Robson, P. Pilesjo (1998), On the ground estimation of vegetation cover in Australian rangelands, *International Journal of Remote Sensing*, 19, No. 9, 1815–1820, **Crossref**

---

**Corresponding author:**

Al-shateri Hoshmand Ahmed Azeez, GIS & Cartography Lecturer at Kalar technical college, Sulaimani Polytechnic University, department of surveying. Sulaimani, Kurdistan-Iraq. ([hoshmendg@gmail.com](mailto:hoshmendg@gmail.com))